Cryogenics 142 (2024) 103918

Contents lists available at ScienceDirect

Cryogenics

journal homepage: www.elsevier.com/locate/cryogenics

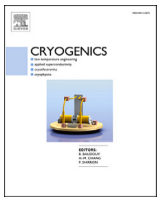

Thermal expansion calculation using FBGS in cryogenic applications

M. Gonzalez [a,b,*], J.M. Martinez Olmo [a], F. Terroba [a], F. Cabrerizo [a], A. Turon [c], J. Renart [c], M. Frövel [a]

[a] Instituto Nacional de Tecnica Aeroespacial (INTA), Carretera de Ajalvir km 4, Torrejon de Ardoz, 28850, Madrid, Spain
[b] Escuela Internacional de Doctorado, Universidad Nacional de Educación a Distancia (UNED), Calle de Bravo Murillo, 38, Madrid, 28015, Madrid, Spain
[c] University of Girona, AMADE, Polytechnic School, Av. Montilivi, Girona, 17003, Catalonia, Spain

ARTICLE INFO

Keywords:
Thermal expansion
Cryogenic temperatures
Liquid helium
FBGS

ABSTRACT

This study presents the measurement of the thermal expansion of aluminum alloy 6061 at cryogenic temperatures using Helium as the cooling medium. Three distinct tests were conducted to evaluate thermal expansion: two with gradual and natural heating of the material, and a third with temperature stabilization at key points. Measurements were carried out using Fiber Bragg Grating Sensors (FBGS), which provided precise and reliable data on the material's thermal behavior. The obtained results were compared with reference curves from the National Institute of Standards and Technology (NIST), showing good agreement and validation of the employed methods. This research highlights the effectiveness of using FBGS in measuring thermal expansion under cryogenic conditions and the importance of heating procedures in obtaining accurate data.

Symbols

λ_B	Bragg wavelength (nm)
n_{eff}	effective refractive index
Λ	Grating period
T	Temperature
$\Delta\lambda$	Bragg wavelength variation from a reference wavelength λ_0
λ_0	Wavelength Reference
ε_f	Strain in the fiber
ε_{Al}	Strain in the Aluminum specimen
α_s	Thermo-optic coefficient
α_{glass}	Glass Thermal Expansion coefficient
k_ε	Fiber gauge factor
$\varepsilon^{NIST}_{ref=T_{ref}}(T)$	NIST curve strain function with temperature considering a reference temperature of T_{ref}

Abbreviations

FBG	Fiber Bragg Grating
NIST	National Institute of Standards and Technology
CTE	Coefficient of Thermal Expansion
IVC	Inner Vacuum Case
OVC	Outer Vacuum Case
CT	Cryogenic Temperature (20 K)
RT	Room Temperature (293 K)
INTA	Spanish Aerospace Technical Institute

1. Introduction

Cryogenic thermal expansion is a very important variable to be measured for industrial proposes like for Liquid Hydrogen tanks. The temperatures inside a Hydrogen storage tank oscillate between 4 K and 70 K, and it can provoke high thermal fatigue loads that initiates cracking [1]. Ensuring a low permeability is a very important issue so minimizing cracking is one of the main goals in hydrogen design. Thermal expansion is one important variable for controlling the thermal fatigue provoked by constant temperature changes. There are many thermal expansion curves of different standardized materials by NIST [2] but the use of composite materials in Composite Overwrapped Pressure Vessels (COPVs) has made the thermal expansion measurement more important in recent years.

The main goal of this article is not so much to determine the expansion coefficient of an aluminum allow but to demonstrate that optic fiber is a suitable option to measure thermal expansion or strains in many kinds of materials. There exist many methods to measure the thermal expansion in a metal [3]. Normally, to measure the expansion coefficients, a dilatometer device is used [4], but those types of equipment

* Corresponding author.
E-mail address: gonzalezvm@inta.es (M. Gonzalez).

https://doi.org/10.1016/j.cryogenics.2024.103918
Received 11 June 2024; Received in revised form 1 August 2024; Accepted 1 August 2024
Available online 6 August 2024

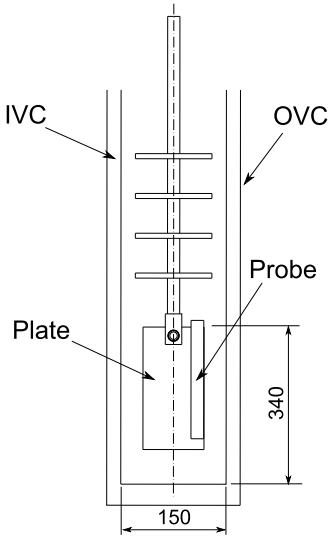

Fig. 1. Cryostat Assembly diagram. IVT: Inner Vacuum Case. OVT: Outer Vacuum Case.

suit better to scientific installations. In the case of INTA the dilatometer is a complex device to be introduced in a tensile test cryostat so different methods to measure the CTE at low temperatures were considered. Nowadays the quartz dilatometer method is the most extended because it is very highly precise [5,6]. For CTE measurement in very low temperatures (below 50 K), capacitive sensors could be used as well [7] but they require specific equipment that should be introduced in the cryostat as well.

One typical solution seen in the bibliography [8–10] is using thermally compensated strain gauges to measure the thermal expansions of metals. This solution could be practical and easy to implement even though the method has not been used widely and not references were found in which this method was used for measuring thermal expansion in temperatures between 1 and 20 K. Many problems could emerge from measuring thermal expansion with those kinds of methods such as temperature control or ensuring temperature spatial uniformity. In the literature, thermal temperature control systems are commonly used for ensuring a feasible temperature distribution in all the probes [11].

The use of optic fiber in cryogenic applications can be a good method to substitute the strain gauge and its problems. Strain gauges have high gauge factor variations with temperature. Moreover, using electrical connections in Cryogenic Temperatures can be tedious. In reference [12] there is a detailed thesis about the measurement of strains and temperatures for cryogenic applications. It has been common to use palladium tubes or coatings in combination with Fiber Bragg gratings in references [13,14]. To measure strains, some FBGS-based extensometers have been designed and are currently on the market but they commonly have operative temperatures above -20ºC, so they cannot be used in cryogenic applications. FBGS have been used for strain measurement many times, with optimal results like in reference [15].

2. Materials and methods

2.1. Test description

The tests were carried out in INTA OXFORD cryostat, model 100KN, S/N 40786 in the frame of the project Cryfto. The mechanical and thermo-mechanical properties of the aluminum alloy (6061) are known using the NIST database [16] in the range between 18 K and Room Temperature. The NIST data is going to be taken as a reference for the new mechanical properties' calculation. In Fig. 1 is reported the cryostat showing that the interior does not allow placing a dilatometer, and all the parts used for the test.

Table 1
Temperature slopes during the cycles.

Cycle	Maximum temperature slope (K/min)	Average temperature slope (K/min)
1	1.01	0.45
2	1.09	0.37
3	1.07	0.44
4	0.99	0.45
5	1.19	0.24

To know the temperature inside the equipment three CERNOX thermoresistive sensors [17] were located inside the cryostat, so the thermal homogeneity in the cryostat could be checked. All sensors were in the air and held to a 7075 Aluminum alloy plate as reported in Fig. 4 in different positions. The CERNOX that was used as a reference was the sensor placed in the center (see sensor 2 in Fig. 4). The CERNOX were connected to an acquisition equipment Lakeshore 218. The Lakeshore was connected by a serial communication to a laptop that measures the temperature data. The aluminum probe was placed on the plate where the sensors are located as reported in Fig. 4. The contact between the plate and the probe was done using aluminum adhesive tape.

Three temperature tests were carried out on different days. The temperature was decreased using firstly Liquid Nitrogen to cool the cryostat to 77 K. Then the Liquid Nitrogen was expelled and Liquid Helium was introduced in the cryostat to cool it to less than 20 K. Once the Cryostat was cooled down, the temperatures raised naturally with very low slopes, so temperature homogeneity was ensured. Normally, in other tests, different methods were used to ensure temperature homogeneity, like for example PID [10]. In this case, due to the vacuum-based thermal isolation of the cryostat, temperature control was unnecessary. In total four repetitions were done during the first test and other repetitions were done during the third test. The fifth repetition was done to see if heating until Room temperature and then cooling to Cryogenic temperatures could have affected the results. The mean and maximum values of the heating temperature slope are reported in Table 1.

Finally, the last test was done by stabilizing the temperature with a temperature control system like in reference [10] for a certain dwell time, so the accuracy is maximized. In the last cycle, only the temperatures after a certain stabilization time were considered. The temperature in the sensor that is in the plate top part (CERNOX 3) is higher due to the lower density of incoming Gas Helium or Nitrogen. Therefore, the temperature was not homogeneous in all the aluminum probes, but the errors were minimal for the tested temperatures (± 1 K). In the aluminum, the probe was partially bonded to one optical fiber. The fiber has four different gratings with a spectrum at Room and Cryogenic temperatures as in Fig. 3. The spectrum has the three first peaks with a high power reflected. The last peak has a lower peak reflection due to damage in the fiber done during the handling. The gratings that correspond to the two first peaks (1520 nm and 1525 nm) are bonded to the probe using a common bicomponent epoxy adhesive (X60 HBK [18]). The fiber was completely covered by the adhesive in the bonded surface so the strain transition is maximized as reported in reference [19]. The fiber was glued using a mold made of non-stick material, and then the assembly was cured by applying pressure to the area with adhesive. The two last gratings are stress-free (see Fig. 4) so the thermal compensation could be done (see section 2.3). The coating selected for the optical fiber was polyimide, manufactured with the FemtoSecond Grating technology [20] (FiSens Ultra High Strength, Reflectivity > 25% UHS25).

The coating of the stress-free gratings was removed thermally by burning the coating, and then the coating rests were removed using an alcoholic solution. The burning method was adopted because it is easy to implement, incurs lower costs compared to other procedures, and reduces the risk of fiber rupture associated with using a mechanical method with a fiber optic stripper. As it was specified previously during that process the last grating was partially broken decreasing its reflected

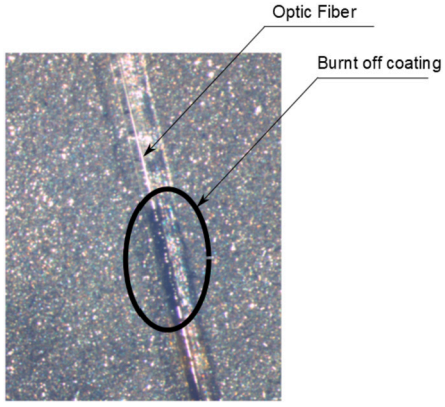

Fig. 2. Optical microscope (X3.2) snapshot of the optical fiber. A light source was oriented to force fiber light reflection.

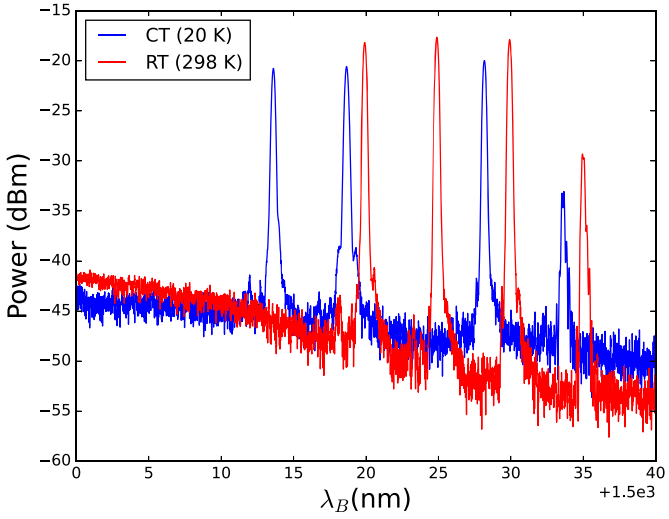

Fig. 3. FBGS spectral response. Channel 1 according to Table 2.

power. The coating of the other grating was not totally removed so the coating residual had an influence on the temperature measurement of the grating. The polyimide coating was removed through local burning, with a posterior alcohol cleaning. In Fig. 2 a microscope snapshot is reported, focused in the third grating illuminating such that the optical fiber reflects the light. The image clearly shows remnants of the burnt coating that was not effectively removed.

In the third test, an additional Optic Fiber was added to the other Probe's face. The same kind of fiber as in the two previous tests was used, with a polyimide coating, but this time with five inscribed gratings. In this case, the coating in the gratings 6, 7, 8, and 9 was removed using Sulfuric acid, to avoid burnt-off coating rests like in the other fiber as seen in Fig. 4. The gratings 5, 6, and 7 were bonded to the probe surface using the X60 adhesive, and the 8 and 9 gratings were stress-free (refer to the diagram in Fig. 4). This fiber was connected to the second channel, and the previous one was connected to the first channel as reported in Table 2.

2.2. Data acquisition

The optic Fiber was connected to a LUNA Si155 interrogator [21]. The interrogator was connected as well through an Ethernet TCP/IP connection to the same laptop in which the Lakeshore equipment is connected with a Serial RS-232 connection. The data acquisition software was done by a Python script that on the one hand takes the serial data from the Lakeshore and on the other hand takes the peak data from the SI155. The peak data taken from Si155 has a sampling frequency

Table 2
Characteristic wavelengths.

Channel	Sensor name	Wavelength (nm)
1	FBG_1	1519.791
	FBG_2	1524.769
	FBG_3	1529.861
	FBG_4	1534.937
2	FBG_5	1519.864
	FBG_6	1525.001
	FBG_7	1529.956
	FBG_8	1535.023
	FBG_9	1540.031

of 10 Hz but the data is saved each two seconds using a moving average. The Lakeshore equipment sampling time is one second. There is a second subprocess that takes the spectrum data plots it and saves each minute the spectrum data in a text file which name is the timestamp when the spectrum was acquired. Spectrum saving was done, because many times if it exists a high transversal strain, there could be peak splitting [22]. Another factor that underscores the importance of spectrum saving is adhesive debonding, which induces a strain gradient in the grating, leading to an increase in peak width [23,24].

2.3. Mathematical and physical formulation

Firstly, the relationship between the optical measured variable (Bragg wavelength) and the physical variable has to be established. The relationship between the Bragg wavelength and the grating period is:

$$\lambda_B = 2n_{eff}\Lambda \tag{1}$$

Differentiating the previous equation with the longitude and the temperature we get [22]:

$$\Delta\lambda_B = 2\left[\left(\Lambda\frac{\delta n_{eff}}{\delta l} + n_{eff}\frac{\delta\Lambda}{\delta l}\right)\Delta l + \left(\Lambda\frac{\delta n_{eff}}{\delta T} + n_{eff}\frac{\delta\Lambda}{\delta T}\right)\Delta T\right] \tag{2}$$

Considering the variation of the Bragg wavelength compared with its initial value [22]:

$$\begin{cases} \frac{\Delta\lambda_B}{\lambda_0(T=18K)} = k_\varepsilon\varepsilon_f + \alpha_s\Delta T \\ \varepsilon_f = \varepsilon_{Al} + \alpha_{glass}\Delta T \\ \varepsilon_{Al} = C^{-1}\sigma + \alpha_{Al}\Delta T \end{cases} \tag{3}$$

The external forces in the probe are null so the term $C^{-1}\sigma$ is null in equation (3). The main goal is to isolate the thermal aluminum strain ε_{Al} from equation (3). Knowing that the last grating is free of the aluminum strains ($\varepsilon_{Al} = 0$), the following expression could be formulated:

$$\left.\frac{\Delta\lambda_B}{\lambda_0(T=18K)}\right|_{bonded} - \left.\frac{\Delta\lambda_B}{\lambda_0(T=18K)}\right|_{free} = (k_\varepsilon\varepsilon_{Al} + k_\varepsilon\alpha_{glass}\Delta T + \alpha_s\Delta T) - (k_\varepsilon\alpha_{glass}\Delta T + \alpha_s\Delta T) = k_\varepsilon\varepsilon_{Al} \tag{4}$$

2.4. NIST curve

The NIST database contains information about the deformation caused by thermal expansion in the temperature range between 0 and 295 K. The data is presented with a quadric curve that was fitted by NIST and has the following parameters:

$$[(L - L_{293}/L_{293}]10^5 = -4.1310^2 - -0.304T + 8.7710^{-3}T^2 - 9.9810^{-6}T^3$$
$$295K > T > 18K \tag{5}$$

The thermal expansion deformation is constant under 18 K. This curve is going to be used as a reference in order to check if an FBGS could

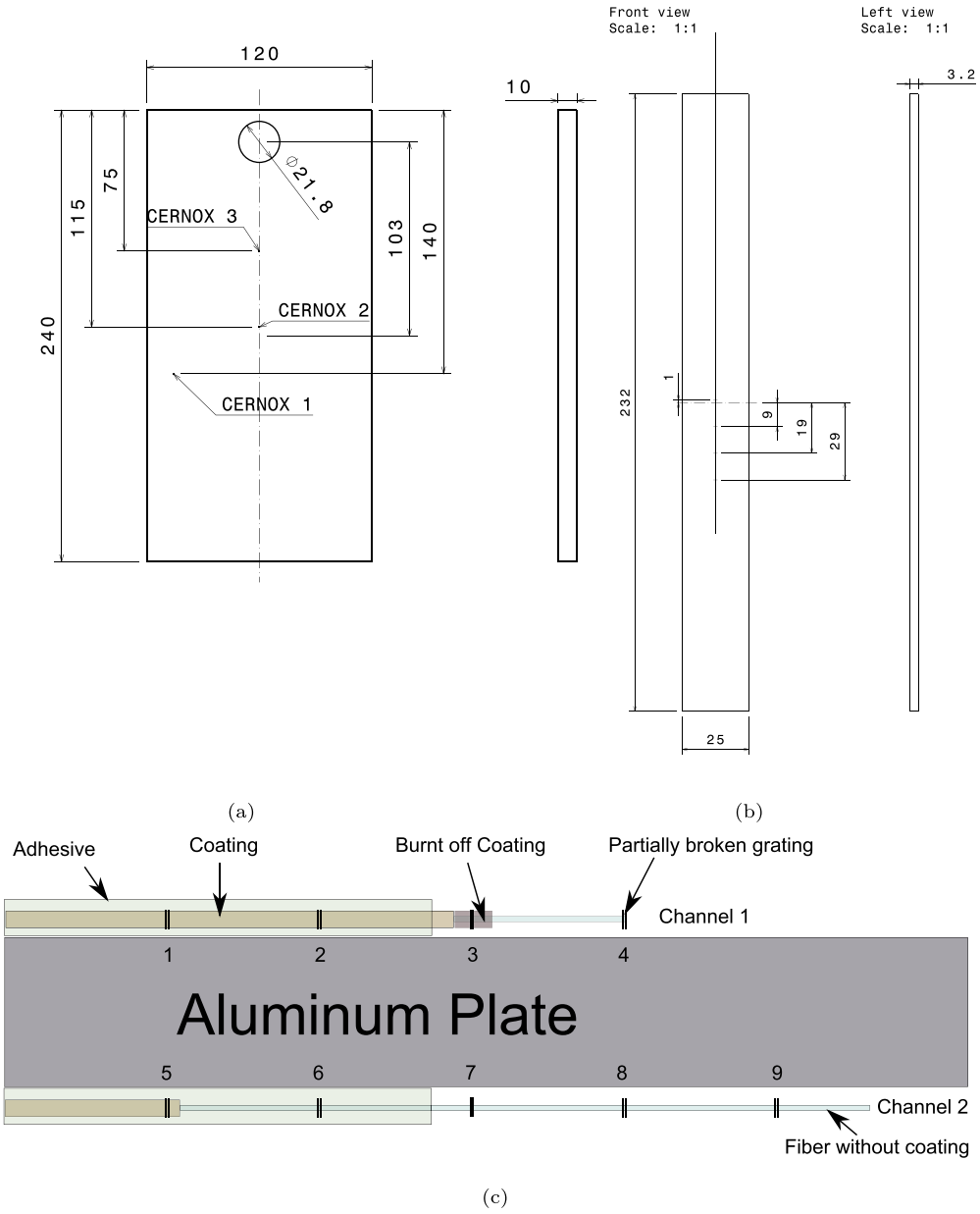

Fig. 4. Diagram with the positions of the sensing points. a) Probe b) plate c) Scheme.

be used as a thermal expansion sensor. Normally, the thermal expansion deformations are expressed using the 298 K reference temperature. To have a clearer value, a change in the reference temperature could be made:

$$\varepsilon^{NIST}_{ref=20K}(T) = \frac{\varepsilon^{NIST}_{ref=298K}(T) - \varepsilon^{NIST}_{ref=298K}(T=20K)}{1+\varepsilon^{NIST}_{ref=298K}(T=20K)} \tag{6}$$

3. Results and discussion

3.1. Tests 1 and 2 thermal expansion measurement

Firstly, the expression $\frac{\Delta\lambda_B}{\lambda_0(T=18K)}$ of each sensor was calculated and plotted against the temperature. In Fig. 5 is seen that the curves of the two first sensors have more slope than the other ones due to the strain caused by the expansion of the probe during heating. The third sensor has a higher slope than the fourth sensor because, as it has been mentioned in section 2.1, the fiber coating was not totally removed. For that reason, the fourth sensor was taken as a reference. The fourth sensor has a higher Signal to Noise ratio probably because part of the grating was broken during fiber handling when it was placed on the probe.

Then, according to equation (4) we get the value of deformation provoked by thermal expansion strain with the expression, being "i" the number of the grating and knowing that the fourth grating is the reference:

$$\varepsilon^{i}_{Al} = \frac{1}{k_\varepsilon}\left(\frac{\lambda^i - \lambda^i_0}{\lambda^i_0} - \frac{\lambda^4 - \lambda^4_0}{\lambda^4_0}\right) \quad for \;\; i = 1,2 \tag{7}$$

The strain values of the first and fourth sensors were plotted to know how the NIST curve fitted with the experimental data. In the NIST curves the reference L0 was taken at 298 K (see section 2.4) but the reference temperatures were changed, firstly to 18 K and for the second test to 23 K using equation (6). The fiber strain constant was 0.78 like in other references [12,24–28]. If the data from the NIST curve and the experimental data are plotted in the same figure so they can be easily compared: The

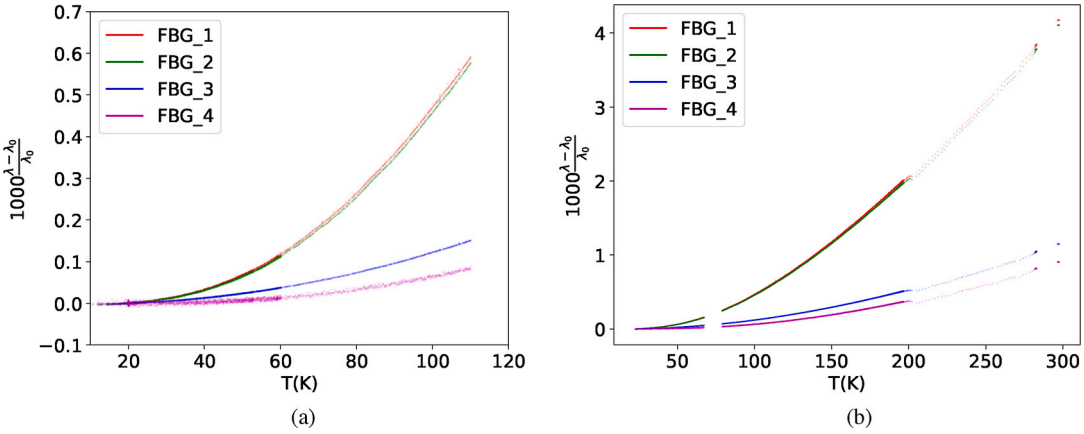

Fig. 5. Wavelength variation with temperature in all the gratings.a) Test 1 b) Test 2.

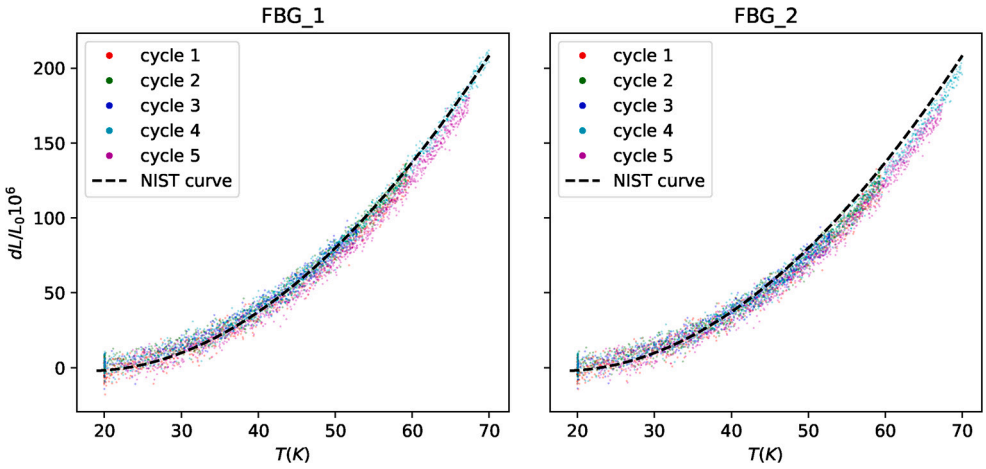

Fig. 6. Expansion curves with temperature. The first four cycles belong to the first test and the fifth cycle to the second test with slow temperature increments.

Table 3
Coefficient of determination of the different Tests.

Cycle	Temperature Interval (K)	Grating Name	R2
Test 1	0-70	FBG_1	0.99991
		FBG_2	0.99992
Test 2	0-70	FBG_1	0.99911
		FBG_2	0.99913
Test 3	0-100.4	FBG_1	0.995093
		FBG_2	0.998872
		FBG_5	0.99290
		FBG_6	0.99850
		FBG_7	0.99827

coefficient of determination R2 values compared with NIST curve is reported in Table 3 and has been calculated:

$$R^2 = 1 - \frac{\sum_i \varepsilon_i^s - \varepsilon_i^{NIST}}{\sum_i \varepsilon_i^s - \bar{\varepsilon^s}} \tag{8}$$

In the case of the last cycle, the fitting R square value is lower probably because during the heating in lower temperatures, the temperature increase slope was higher, so there was less dwell time.

It can be seen in Fig. 6 that the fifth thermal cycle is slightly different than the previous ones and there is a difference with the NIST curve. The curve in the fifth cycle has lower wavelengths associated with the same temperatures. This may be provoked by the higher heating slope in the second test than in the four repetitions of the first test. Higher slopes mean that the temperature of aluminum does not have enough time for heating and the real temperature of aluminum is lower than the real one, measured by the three CERNOX. In the lower temperatures that fact is not as important because the thermal capacity of solids tends to zero at temperatures close to absolute zero [29]. Another possibility is that between test 1 and test 2, the sensor was heated to Room Temperature and then cooled again to Cryogenic temperatures. That thermal difference could have provoked microcracking in the interphase reducing the strain transmission.

The other aspect that has been considered crucial is evaluating if there is repetitiveness in the Bragg Wavelength with temperature. In the first four cycles, the wavelength associated with low temperatures is very repetitive, with a wavelength of 1513.604±1e-3 nm in the first grating and 1518.664 ± 1e-3 nm in the second one associated with a temperature of 20 K. On the other hand, in the last cycle associated with the second test, there is a large wavelength change of 1513.509 nm and 1518.648 nm for a temperature associated with 22 K. That high wavelength change could be caused by FBGS coating cracking or cracking of the adhesive provoked by a very high-temperature change between the first test and the second one. This fact implies that it may be convenient to conduct tests with smaller thermal variations, for example, testing only within a specific thermal range, or that it may be convenient to perform the test only once. Nevertheless, it can be observed that despite this change in wavelengths, the results in the last repetitions are also satisfactory.

3.2. *Test 3 thermal expansion measurement*

In the test, as reported in section 2.1, the temperatures were controlled and a dwell time was set. The dwell time for each temperature

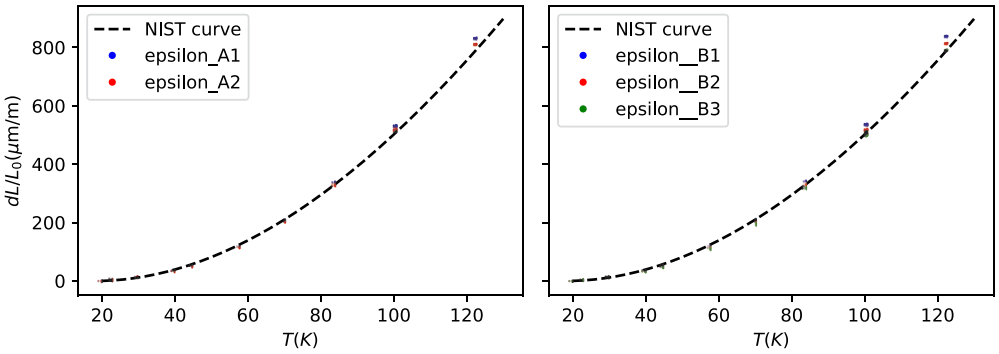

Fig. 7. Thermal expansion read by the two different FBGS (channel 1 on the left side and channel 2 on the right side) in a test with temperature stabilization.

Table 4
Dwell times and standard deviation of the different temperatures in test 3.

Temperature (K)	Dwell Time	Standard Deviation(K)
19,81	01:14	0,25
22,79	01:43	0,15
29,71	01:45	0,16
39,84	01:21	0,25
44,73	02:03	0,12
57,67	0:47	0,13
70,13	01:53	0,05
83,79	02:25	0,2
100,54	08:00	0,19

can be seen in Table 4. This test had two main goals, the first one was to validate the models previously applied in tests 1 and 2, and to test if there is any effect of the coating in the results. The R^2 is lower than the previous tests, probably due to the quantity of data in the same dwell time, but the curve and the data have a very strong correlation (see Table 3). The polyimide coating did not have any important effect on the results and it was seen that all the curves have similar results.

A significant potential source of error lies in the temperature distribution within the sample space. Fig. 7 displays results obtained using equation 10, revealing that sensors 1 and 5 exhibit higher strains compared to sensors 2, 6, and 7. This discrepancy may arise from the former sensors being positioned at a greater height, thus experiencing higher temperatures than those recorded by the CERNOX sensor. A comparison between the outcomes in Fig. 7 and Fig. 6, coupled with insights from Table 3, underscores the consistency of results at lower temperatures, regardless of dwell time or gradual temperature increments.

4. Conclusions

Two distinct testing methodologies were employed, each yielding exact results. The initial approach involved a gradual heating process, while the subsequent method focused on maintaining temperature stability over a specified duration. The strain results were monitored with several Fiber Bragg Grating sensors, so the strain and temperature homogeneity were studied in both probe faces.

A total of six different cycles were tested. The first five cycles involved very slow heating, while the last cycle involved stabilizing the temperature at various levels. Numerous repetitions were performed to ensure consistent results. The test outcomes were satisfactory, indicating a congruence between the FBGS strain values and the NIST curve. Notably, FBGs exhibited commendable efficacy in measuring strain even under extremely low-temperature conditions. The sensor response was accurate regardless of whether it had a coating.

These tests aimed to validate a testing methodology for future thermal expansion testing of composite materials, a topic of significant interest. This validation was particularly crucial just before the beginning of the Composite Material test campaign in the frame of the project CRYFTO. Given the complexities of composite materials, such as the potential presence of higher transversal strains during testing, additional precautions must be considered, like spectrum saving and postprocessing to see possible peak splitting or widening.

Another issue observed during the tests is the fragility of the fiber compensation gratings due to the removal of their coating. Having a coating would facilitate handling the fiber during adhesion, but its presence leads to inaccurate results, making coating removal mandatory (see FBG_3 from tests 1 and 2 in Fig. 5). One solution is to determine the wavelength variation from other tests in advance and use the CERNOX-measured temperature for compensation. Another option is to understand the coating effect and, using a coated fiber, apply compensation for that effect.

Extended dwell times are not essential when measuring thermal expansion strains in low temperatures. Accuracy can be achieved if the probe temperature changes gradually due to the low thermal capacity of the material at cryogenic temperatures. However, ensuring temperature homogeneity within the testing area is crucial to minimize errors. Therefore, care should be taken during tests, and an investigation of thermal homogeneity is necessary to ensure data accuracy.

Funding

This work has been partially funded by the Spanish Government (Ministerio de Ciencia e Innovación) under contracts PID2021-127879OB-C21 and PID2021-127879OA-C22.

CRediT authorship contribution statement

M. Gonzalez: Writing – review & editing, Writing – original draft, Visualization, Software, Methodology, Investigation, Funding acquisition, Data curation. **J.M. Martinez Olmo:** Validation, Supervision, Investigation, Formal analysis, Conceptualization. **F. Terroba:** Validation, Supervision, Conceptualization. **F. Cabrerizo:** Supervision, Conceptualization. **A. Turon:** Writing – review & editing. **J. Renart:** Writing – review & editing. **M. Frövel:** Validation, Supervision, Investigation, Formal analysis, Conceptualization.

Declaration of competing interest

The authors declare that they have no known competing financial interests or personal relationships that could have appeared to influence the work reported in this paper.

Data availability

Data will be made available on request.

Acknowledgements

AT acknowledges the Generalitat de Catalunya for the ICREA Academia Prize 2022.

References

[1] Kim RY, Donaldson SL. Experimental and analytical studies on the damage initiation in composite laminates at cryogenic temperatures. Compos Struct 2006;76:62–6. https://doi.org/10.1016/j.compstruct.2006.06.009. https://linkinghub.elsevier.com/retrieve/pii/S0263822306002492.

[2] Cryogenic Materials Properties Reference List, https://www.nist.gov/mml/acmd/cryogenic-materials-properties-reference-list, 2018. last Modified: 2021-06-02.

[3] Test Standard. Method for linear thermal expansion of solid materials by thermomechanical analysis ASTM E831-19 https://www.astm.org/e0831-19.html.

[4] Kroeger FR, Swenson CA. Absolute linear thermal-expansion measurements on copper and aluminum from 5 to 320 K. J Appl Phys 1977;48:853–64. https://doi.org/10.1063/1.323746. https://pubs.aip.org/jap/article/48/3/853/506194/Absolute-linear-thermal-expansion-measurements-on.

[5] Clark A. Low temperature thermal expansion of some metallic alloys. Cryogenics 1968;8:282–9. https://doi.org/10.1016/S0011-2275(68)80003-7. https://linkinghub.elsevier.com/retrieve/pii/S0011227568800037.

[6] Tezvergil A, Lassila LV, Vallittu PK. The effect of fiber orientation on the thermal expansion coefficients of fiber-reinforced composites. Dent Mater 2003;19:471–7. https://doi.org/10.1016/S0109-5641(02)00092-1. https://linkinghub.elsevier.com/retrieve/pii/S0109564102000921.

[7] White GK, Collins JG. Thermal expansion of copper, silver, and gold at low temperatures. J Low Temp Phys 1972;7:43–75. https://doi.org/10.1007/BF00629120. http://link.springer.com/10.1007/BF00629120.

[8] Finke TE, Heberling TG. Determination of thermal-expansion characteristics of metals using strain gages: a method is described in which bonded resistance strain gages are used to measure temperature-induced length changes in metals. Exp Mech 1978;18:155–8. https://doi.org/10.1007/BF02324149. http://link.springer.com/10.1007/BF02324149.

[9] Measurement of Thermal Expansion Coefficient Using Strain Gage. Technical Report TN-513-1, Micro-Measurements.

[10] Tang K, Sha L, Li Y-j, Jin T, Liu S-j. Measurement of thermal expansion at low temperatures using the strain gage method. J Zhejiang Univ Sci A 2014;15:323–30. https://doi.org/10.1631/jzus.A1400051. http://link.springer.com/10.1631/jzus.A1400051.

[11] Valentich J. Thermal expansion of solids from -261C to 173 C using strain gauges. Cryogenics 1985;25:63–7. https://doi.org/10.1016/0011-2275(85)90105-5. https://linkinghub.elsevier.com/retrieve/pii/0011227585901055.

[12] Frövel M. Sensores de fibra óptica tipo redes de Bragg embebidos en material compuesto para medir deformaciones y temperaturas criogénicas. PhD Thesis. Universidad Politécnica de Madrid; 2006. http://oa.upm.es/459/.

[13] Buric M, Chen KP, Bhattarai M, Swinehart PR, Maklad M. Active fiber Bragg grating hydrogen sensors for all-temperature operation. IEEE Photonics Technol Lett 2007;19:255–7. https://doi.org/10.1109/LPT.2006.888973. http://ieeexplore.ieee.org/document/4079670/.

[14] Aleixandre M, Corredera P, Hernanz M, Sayago I, Horrillo M, Gutierrez-Monreal J. Study of a palladium coated Bragg grating sensor to detect and measure low hydrogen concentrations. In: 2007 Spanish conference on electron devices. Madrid, Spain: IEEE; 2007. p. 223–5. http://ieeexplore.ieee.org/document/4271210/.

[15] Mizutani T, Takeda N, Takeya H. On-board strain measurement of a cryogenic composite tank mounted on a reusable rocket using FBG sensors. Struct Health Monit 2006;5:205–14. https://doi.org/10.1177/1475921706058016. http://journals.sagepub.com/doi/10.1177/1475921706058016.

[16] Aluminum 6061-T6 (UNS AA96061), NIST (2018). URL. https://www.nist.gov/mml/acmd/aluminum-6061-t6-uns-aa96061. last Modified: 2021-06-02T18:27-04:00.

[17] Lakeshore. Cernox® technical specifications. https://www.lakeshore.com/products/categories/overview/temperature-products/cryogenic-temperature-sensors/cernox.

[18] X60 Cold Curing Glue for Strain Gauge Installations. https://www.hbm.com/en/2961/x60-2-component-fast-curing-adhesive/, 2022.

[19] Trutzel MN, Wauer K, Betz D, Staudigel L, Krumpholz O, Muehlmann H-C, et al. Smart sensing of aviation structures with fiber optic Bragg grating sensors. Newport Beach, CA. 2000. p. 134. http://proceedings.spiedigitallibrary.org/proceeding.aspx?doi=10.1117/12.388099.

[20] Davis KM, Miura K, Sugimoto N, Hirao K. Writing waveguides in glass with a femtosecond laser. Opt Lett 1996;21:1729. https://doi.org/10.1364/OL.21.001729. https://opg.optica.org/abstract.cfm?URI=ol-21-21-1729.

[21] LUNA. Si155 datasheet. https://lunainc.com/sites/default/files/assets/files/data-sheets.

[22] Van Steenkiste RJ, Springer GS. Strain and temperature measurement with fiber optic sensors. Lancaster, Pa: Technomic Pub. Co; 1997.

[23] Matveenko V, Serovaev G, Kosheleva N, Galkina E. Investigation of fiber Bragg grating's spectrum response to strain gradient. Procedia Structural Integrity 2024;54:218–24. https://doi.org/10.1016/j.prostr.2024.01.076. https://linkinghub.elsevier.com/retrieve/pii/S2452321624000763.

[24] Peters K, Studer M, Botsis J, Iocco A, Limberger H, Salathé R. Embedded optical fiber Bragg grating sensor in a nonuniform strain field: measurements and simulations. Exp Mech 2001;41:19–28. https://doi.org/10.1007/BF02323100. http://link.springer.com/10.1007/BF02323100.

[25] Zhang X. Strain dependence of fiber Bragg grating sensors at low temperature. Opt Eng 2006;45:054401. https://doi.org/10.1117/1.2202642. http://opticalengineering.spiedigitallibrary.org/article.aspx?doi=10.1117/1.2202642.

[26] Jülich F, Aulbach L, Wilfert A, Kratzer P, Kuttler R, Roths J. Gauge factors of fibre Bragg grating strain sensors in different types of optical fibres. Meas Sci Technol 2013;24:094007. https://doi.org/10.1088/0957-0233/24/9/094007. https://iopscience.iop.org/article/10.1088/0957-0233/24/9/094007.

[27] Hill K, Meltz G. Fiber Bragg grating technology fundamentals and overview. J Lightwave Technol 1997;15:1263–76. https://doi.org/10.1109/50.618320. http://ieeexplore.ieee.org/document/618320/.

[28] Kersey A, Davis M, Patrick H, LeBlanc M, Koo K, Askins C, et al. Fiber grating sensors. J Lightwave Technol 1997;15:1442–63. https://doi.org/10.1109/50.618377. http://ieeexplore.ieee.org/document/618377/.

[29] Barron RF, Nellis G. Cryogenic heat transfer. second edition ed. Boca Raton: CRC Press, Taylor & Francis Group; 2016.